Journal of Power Sources 195 (2010) 2301–2309

Contents lists available at ScienceDirect

Journal of Power Sources

journal homepage: www.elsevier.com/locate/jpowsour

Temperature and stress induced changes of the vibrational response of cubic and rhombohedral 10 mol%Sc_2O_3–1 mol%CeO_2–ZrO_2 ceramics

Svetlana Lukich, Cassandra Carpenter, Nina Orlovskaya*

Department of Mechanical, Material and Aerospace Engineering, University of Central Florida, 4000 Central Florida Blvd., Orlando, FL 32816, United States

ARTICLE INFO

Article history:
Received 13 September 2009
Received in revised form 17 October 2009
Accepted 19 October 2009
Available online 11 November 2009

Keywords:
Micro-Raman spectroscopy
Cubic phase
Rhombohedral phase
Zirconia
Vickers indentation
Stress

ABSTRACT

The vibration response of cubic and rhombohedral (β) 10 mol%Sc_2O_3–1 mol%CeO_2–ZrO_2 ($Sc_{0.1}Ce_{0.01}ZrO_2$) both at room and high-temperatures is reported. The in situ heating experiments and ex situ indentation experiments were performed to characterize the vibrational behavior of these important materials. A temperature and stress-assisted phase transition from cubic to rhombohedral phase was detected during in situ Raman spectroscopy experiments. While heating and indentation experiments performed separately did not cause the transition of the cubic phase into the rhombohedral structure under the performed experimental conditions and only broadened or strained peaks of the cubic phase could be detected, the heating of the indented (strained) surface leaded to the formation of the rhombohedral $Sc_{0.1}Ce_{0.01}ZrO_2$. Both temperature range and strained zone were estimated by in situ heating and 2D mapping, where a formation of rhombohedral or retention of cubic phase has been promoted.

1. Introduction

Sc_2O_3 doped ZrO_2 ($ScZrO_2$) ceramics have recently attracted a significant interest as a novel promising electrolyte material for lower temperature SOFCs due to its excellent ionic conductivity [1–3]. There have been numerous reports on the high ionic conductivity of $ScZrO_2$ ceramics [4,5] which was reported to be near twice as high as other ZrO_2 based electrolytes [6]. Most of the studies of $ScZrO_2$ ceramics were performed on the materials with 8–12 mol% doping level of Sc_2O_3, where a cubic phase is a main single phase at 700–800 °C operating temperatures. The drawback of $ScZrO_2$ has been also reported as an ordering of vacancies over time, called the aging phenomenon, accompanied by a phase transition to a lower symmetry rhombohedral phase, resulting in decreased conductivity [6]. The highly conductive cubic phase is not stable below 650 °C causing the abrupt decrease in ionic conductivity during cooling in the $ScZrO_2$ [7,8]. It is known that in 11 mol% Sc_2O_3–89 mol% ZrO_2, a cubic to rhombohedral phase transition occurs when the temperature decrease below 600 °C [9,10]. It was reported [11,12] that when ZrO_2 is stabilized with a small amount of CeO_2 along with Sc_2O_3, it no longer exhibits an unfavorable phase transition, making this material a very promising option for intermediate temperature electrolytes.

In [11], the commercially available 10 mol% Sc_2O_3–1 mol% CeO_2–ZrO_2 further referred as $Sc_{0.1}Ce_{0.01}ZrO_2$, manufactured by Daiichi Kigenso Kagaku Kogyo (DKKK, Japan) has been reported to have a stable cubic phase, superior electrical properties and excellent high temperature long-term operating characteristics of single cells using $Sc_{0.1}Ce_{0.01}ZrO_2$ as an electrolyte material. Contrary, the reversible very slow cubic to rhombohedral and rhombohedral to cubic phase transitions at 300–500 °C has been reported upon heating of $Sc_{0.1}Ce_{0.01}ZrO_2$ ceramics using X-ray diffraction [13], which were probably overlooked in other studies due to extremely slow kinetics of cubic to rhombohedral phase transition upon heating. Thus, it was recently shown that the high temperature cubic $Sc_{0.1}Ce_{0.01}ZrO_2$ is a metastable phase at room temperature and could be easily transformed to the thermodynamically stable rhombohedral phase upon annealing at 350–400 °C after at least 12 h of annealing. However, it is not expected that these transitions could have a significant effect on $Sc_{0.1}Ce_{0.01}ZrO_2$ electrolyte performance since they occur at lower temperatures and could simply be bypassed during heating up or cooling down cycles of the cells. It was reported that the kinetics of the phase transition is a strong function of the grain size of the $Sc_{0.1}Ce_{0.01}ZrO_2$ ceramics [13], and it was also found that the coefficient of thermal expansion of cubic $Sc_{0.1}Ce_{0.01}ZrO_2$ is very close to the Y_2O_3 stabilized ZrO_2 (YSZ) which is a good indicator that $Sc_{0.1}Ce_{0.01}ZrO_2$ ceramics are a perfect candidate for substitution of YSZ electrolyte SOFCs.

It has been recognized that while XRD patterns are determined by the arrangements of the cations (Zr, Sc, Ce) in the fluorite lattice, laser-excited Raman spectra are sensitive to the

* Corresponding author. Tel.: +1 4078235770; fax: +1 4078230208.
E-mail address: norlovsk@mail.ucf.edu (N. Orlovskaya).

0378-7753/$ – see front matter © 2009 Elsevier B.V. All rights reserved.
doi:10.1016/j.jpowsour.2009.10.060

change of the polarizability of cation-oxygen vibrations and can easily give important information about the crystal structure of $Sc_{0.1}Ce_{0.01}ZrO_2$. The different ZrO_2 structures (monoclinic, tetragonal, rhombohedral, and cubic) all have characteristic signatures in their spectra, which enable them to be easily distinguished. Besides, the strain/stress in the material can be detected from the shift of the certain peaks. The $Sc_{0.1}Ce_{0.01}ZrO_2$ ceramics under study have been previously characterized by XRD [13], but the goal of this paper is to study the spectra of cubic and rhombohedral phases as well as to detect temperature and stress induced deformation and phase transitions in zirconia using Raman spectroscopy.

2. Experimental details

The 10 mol% Sc_2O_2–1 mol% CeO_2–ZrO_2 ($Sc_{0.1}Ce_{0.01}ZrO_2$) powder produced by Daiichi Kigenso Kagaku Kogyo (DKKK, Japan) has been sintered at 1500 °C for 2 h with a 10 °C min^{-1} heating/cooling rate in air to almost full density. The detailed processing of the $Sc_{0.1}Ce_{0.01}ZrO_2$ as well as it selected properties, such as strength, hardness, fracture toughness, Young's modulus, as well as preliminary Raman data are presented in details elsewhere [13–16]. The XRD confirms that the material consists of the cubic phase upon cooling after sintering at 375 °C for 12 h [13]. The cubic $Sc_{0.1}Ce_{0.01}ZrO_2$ samples were grinded and polished in order to obtain the mirror surface and then they were thermally etched at 1300 °C for 1 h to reveal the grain boundaries. A portion of the thermally etched cubic $Sc_{0.1}Ce_{0.01}ZrO_2$ samples were annealed at 375 °C for 12 h in air in order to convert them to the rhombohedral phase, which is stable in 25–400 °C temperature range [13]. Both cubic and rhombohedral $Sc_{0.1}Ce_{0.01}ZrO_2$ phases were indented using Vickers hardness tester (LECO M-400) with a load of 9.8 N. The hardness and fracture toughness of the ceramics have been calculated using the length of the impression diagonals and cracks originating from the corners of the impressions, respectively. Optical micrographs were taken using an Olympus confocal microscope (LEXT OLS3000-IR).

Renishaw InVia Raman microscope was used to study the vibrational spectra of $Sc_{0.1}Ce_{0.01}ZrO_2$ ceramics. The Raman microscope system comprises a laser (532 nm line of solid Si or near infrared 785 nm) to excite the sample, a single spectrograph fitted with holographic notch filters, and an optical microscope (a Leica microscope with a motorized XYZ stage) rigidly mounted and optically coupled to the spectrograph. Before collecting spectra of $Sc_{0.1}Ce_{0.01}ZrO_2$ the spectrometer was calibrated with a Si standard using a Si band position at 520.3 cm^{-1}. The average collection time for a single spectrum was 20 s. High temperature Raman spectroscopy was performed using a TMS 600 and TMS 1500 heating stage (Linkam Scientific Instruments Ltd., UK) by heating/cooling of the samples to/from 400 and 1000 °C, respectively. For the high temperature experiments the incident and scattered beams were focused with a long working distance 50× objective, which maintained a laser spot as small as 2–3 μm. A 10 °C min^{-1} heating/cooling rate was used for high temperature experiments. Room temperature Raman spectra were collected from different points of interest on the sample surface, such as on the polished surface at different locations as well as inside or outside the Vickers impressions. For room temperature and area mapping experiments the short working distance 100× objective was used. To produce two-dimensional (2D) maps, Renishaw Wire 2.0 software with a mixed Lorentzian and Gaussian peak fitting function was used. The system's peak fitting results were plotted to create a position map with a spectral resolution better than 0.2 cm^{-1}. The total time of spectrum collection was decreased to 3 s per point in the case of 2D mapping and the total acquisition time to collect all spectra for one map never exceeded 24 h.

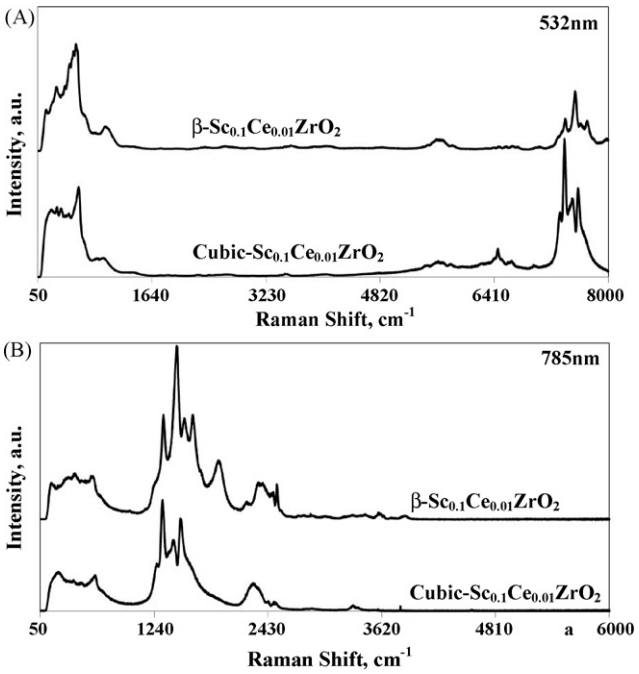

Fig. 1. The spectral range of cubic and rhombohedral $Sc_{0.1}Ce_{0.01}ZrO_2$ electrolyte ceramics collected by 532 nm solid Si and 785 nm NIR lasers.

3. Results and discussion

The whole spectral range of cubic and rhombohedral $Sc_{0.1}Ce_{0.01}ZrO_2$ phases collected using both 532 and 785 nm lasers are presented in Fig. 1. The assignment of the cubic and rhomboherdal phases were made based on the XRD analysis presented elsewhere [13]. While the spectra collected using 532 nm Si laser shows the most prominent features at ranges 100–1000 cm^{-1} and 7200–8000 cm^{-1} both for cubic and rhombohedral structures, the spectra collected using NIR 785 nm laser shows the strongest bands in the 1000–2000 cm^{-1} range. Thus, it is useful to study the vibrational response of the $Sc_{0.1}Ce_{0.01}ZrO_2$ using at least two lasers, as the structural information from the analysis of Raman spectra measured with only one laser could be incorrectly interpreted. A number of peaks showing up both in cubic and rhombohedral $Sc_{0.1}Ce_{0.01}ZrO_2$ in 1000–2000 cm^{-1} range using 785 nm excitation, are completely missing when 532 nm laser is used, Fig. 1. The bands with a Stokes shift higher than 800 cm^{-1} from the laser excitation line have been previously observed in zirconia based oxides [17–19], and bands have been assigned to electronic transitions in impurity ions [20] or to phonon-mediated de-excitation of excited states of the impurity-doped ZrO_2 lattice [21]. While the exact nature of the bands is not obvious, they could be tentatively assigned to the appearance of the luminescence bands related to Ln^{3+} (Ln: Pr^{3+}, Nd^{3+}, Mo^{3+}, Er^{3+}) or other impurities ions [22], and photoluminescence measurements need to be performed to establish the origin of each 1000 cm^{-1} and higher bands.

The spectra of cubic and rhombohedral $Sc_{0.1}Ce_{0.01}ZrO_2$ phases in 100–1000 cm^{-1} range taken by 532 and 785 nm lasers are presented in Fig. 2. The similar spectrum of cubic $Sc_{0.1}Ce_{0.01}ZrO_2$ electrolyte was published in [23]. The spectrum of pure cubic fluorite phase should consist of a single F_{2g} mode between 400 and 500 cm^{-1}, and it was reported that Raman spectrum of pure submicron cubic zirconia consists of a weak broad line assigned to a single allowed Raman mode F_{2g} symmetry [24]. The out-of-phase motion of the 2 oxygen atoms is assigned to this mode, therefore the frequency should be independent of the cation mass, and should vary inversely proportional to the square root of the cell volumes. It

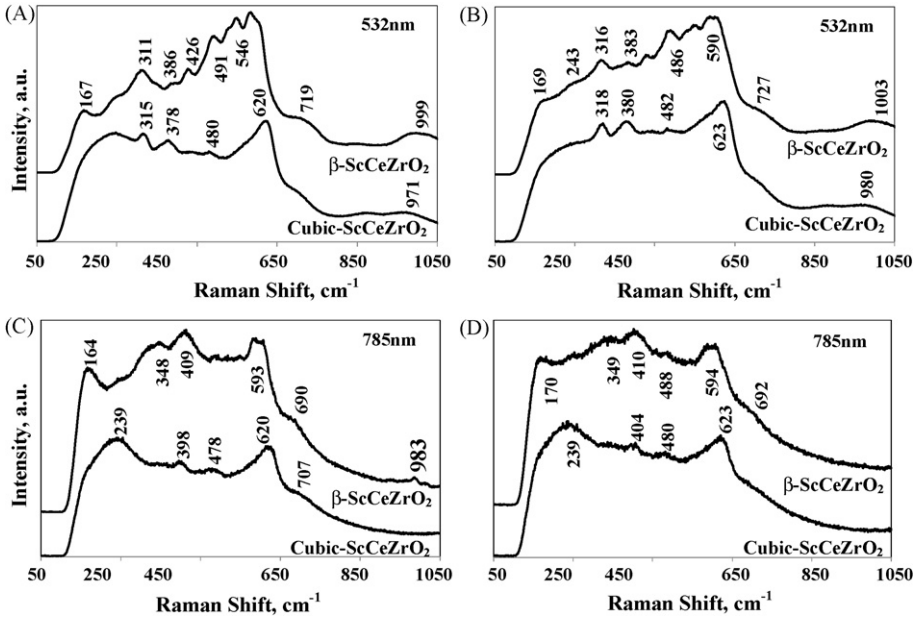

Fig. 2. Vibrational spectra of cubic and rhombohedral (β) $Sc_{0.1}Ce_{0.01}ZrO_2$ ceramics; (A and C) non-deformed polished surface, (B and D) center of Vickers impression.

was reported that in fluorite structures, CeO_2, ThO_2, UO_2 the mode has been observed near the 460–470 cm^{-1} region [25,26]. However, the spectrum of cubic $Sc_{0.1}Ce_{0.01}ZrO_2$ contains a number of bands, and some of the bands at 800 cm^{-1} and below were assigned to Raman active lattice phonons [27,28]. They are located at 239, 478, 480, and 623 cm^{-1} (Fig. 2). At the same time the two bands at 315 and 378 cm^{-1} detected by 532 nm laser were not revealed when spectrum was taken by 785 nm laser, and a band at 398 cm^{-1} was detected by 785 nm laser, but it did not show up in the 532 nm spectrum. Therefore, it is fair to notice that the 315, 378, and 398 cm^{-1} bands do not belong to fluorite lattice vibrations, but might appear due to presence of impurities. The appearance of the peaks, which are not allowed in the cubic fluorite structure, can be also attributed to the disorder of ionic defects in the oxygen sublattice. Substitution of Zr^{4+} by Sc^{3+} results in the formation of high quantities of oxygen vacancies, and such high defect concentration can lead to a violation of the selection rules and allows the appearance of additional modes that are forbidden for the cubic fluorite structure [28]. The possibility of lowering the cubic symmetry on the local scale, which cannot be detected by X-ray diffraction, cannot be excluded, since the oxygen immediately surrounding a vacancy collapse creating structural short range disorder on the oxygen sublattice. It was reported that appearance of the extra peaks, which are not allowed in the cubic fluorite structure, could indicate a presence of lower symmetry t'-phases, which is difficult to distinguish from cubic structure by X-ray diffraction [12,29].

In order to study the effect of stress on vibrational properties of cubic and rhombohedral $Sc_{0.1}Ce_{0.01}ZrO_2$, the polished surface was indented using Vickers diamond indenter. For comparison, the spectra taken both from the non-deformed surface and from the center of the Vickers impressions of cubic and rhombohedral $Sc_{0.1}Ce_{0.01}ZrO_2$ are shown in Fig. 2. While, the position shift and change of the intensities and full width at half maximum (FWHM) of certain bands can be detected, the structures of cubic and rhombohedral phases remain the same after the deformation by the sharp Vickers indenter. The broadening and decrease of the intensities of the bands after indentation are indicative for increased crystalline disorder, e.g. introduction of internal strain and dislocations along with other defects. However, no stress induced phase transformation with detectable localized changes of structure which change selection rules and cause splitting of vibrational modes can be reported upon indentation.

The differences between the cubic and rhombohedral $Sc_{0.1}Ce_{0.01}ZrO_2$ are clearly visible in Fig. 2, especially when spectra are taken using 532 nm Si laser. As it was already reported in [10] the Raman spectrum of rhombohedral phase is rather complex, presented by a characteristic broad continuum with many small peaks rising above background.

The bands of cubic $Sc_{0.1}Ce_{0.01}ZrO_2$ display anharmonic effects as temperature is raised, with broadening and merging of the peaks [30]. The asymmetry of the 623 cm^{-1} band in Fig. 3, on the left low frequency side of the cubic $Sc_{0.1}Ce_{0.01}ZrO_2$ is typical for disordered systems, as it was indicated by Kosacki et al. [28]. The heating of the cubic $Sc_{0.1}Ce_{0.01}ZrO_2$ up to 1000 °C did not remove the asymmetry (Fig. 3), however the intensities of the bands decreased and a significant broadening of the peaks due to anharmonicity, the onset of oxygen diffusion and the increasing dynamic structural disorder of the oxygen sublattice has been observed upon temperature increase. The weak band at 480 cm^{-1}, which could indicate the lowering of the cubic symmetry to tetragonal (*t'*) phase at room temperature [29], completely disappeared upon heating above 500 °C. The asymmetric 623 cm^{-1} band is shifted to the lower wavenumbers, as temperature was increased; however bands 315 and 378 cm^{-1} are shifted to the higher wavenumbers. The position of the first band was located at 315 cm^{-1} at room temperature, but it was shifted to 342 cm^{-1} at 400 °C. Due to the broadening, a 315 and 378 cm^{-1} bands coalesced into one broad band starting from 800 °C, which was impossible to deconvolute into two peaks. Such shift to the higher wavenumber, upon heating is also indicative that the bands are not due to vibrations of the ions in the fluorite lattice. At the same time, two broad bands in 800–1050 cm^{-1} region completely disappeared at 400–500 °C upon heating, but later reappeared when the sample was cooled after heating experiments.

Since the vibrational frequencies of both cubic and rhombohedral $Sc_{0.1}Ce_{0.01}ZrO_2$ are very complex below 800 cm^{-1} (Fig. 2) they are not suitable for the mapping experiments, which can help to detect the phase transitions or identify the distribution of residual stresses. Therefore, the 1000–2000 cm^{-1} range of the spectrum has been chosen for the collection of 2D maps using NIR 785 nm laser. While the origin of the bands is not presently known, however pho-

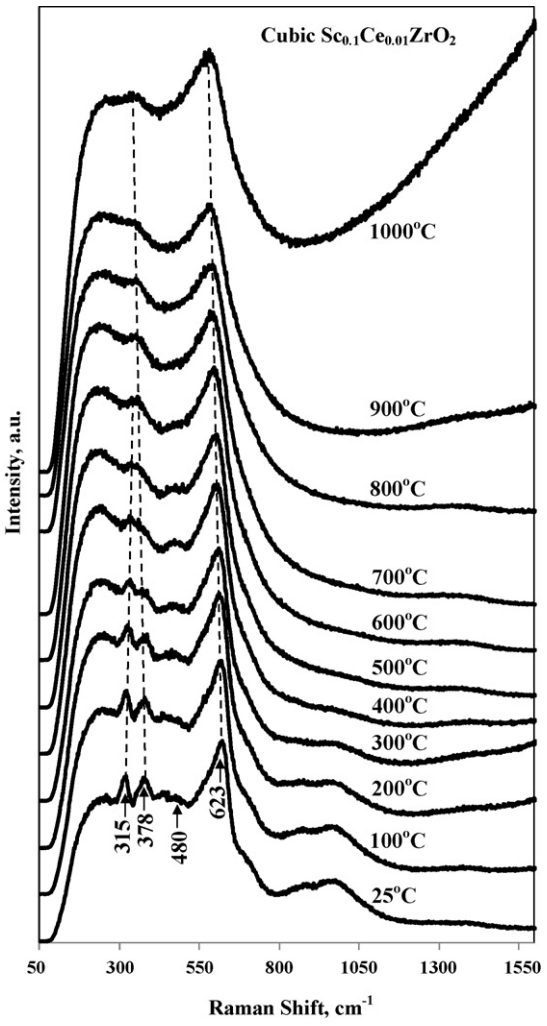

Fig. 3. High temperature spectra of cubic of $Sc_{0.1}Ce_{0.01}ZrO_2$ ceramics heated up to 1000 °C with 100 °C step size and 10 °C min^{-1} heating rate. A dwell time of 5 min was used at each temperature before spectrum's collection.

toluminescence measurements are underway and they will help to identify both the nature of the bands and the nature of the impurities which caused the vibrations. Thought the bands in the 1000–2000 cm^{-1} range do not represent the vibrational response of ions in zirconia lattice, they still can be easily used to identify both the presence of the cubic and rhombohedral phases and help detect residual stress existing in the material due to temperature or pressure effects. The approach is similar to the one used in alumina to detect stresses using well known R-line peak positions which appeared because of the transitions between the ground state of the Cr^{3+} impurity ion and its first excited state, when the material is excited with an citation source such as a laser [31,32].

Fig. 4A represents the typical spectra of cubic and rhombohedral phases. Spectra taken both from the polished surface and from the center of the Vickers impression do not show a significant difference. The deconvoluted peaks of cubic and rhombohedral $Sc_{0.1}Ce_{0.01}ZrO_2$ are shown in Fig. 4B. Confocal optical micrographs of the cubic and rhombohedral $Sc_{0.1}Ce_{0.01}ZrO_2$ are shown in Fig. 5(A and B). While the cubic $Sc_{0.1}Ce_{0.01}ZrO_2$ has a smooth and flat surface, where grain boundaries are clearly visible, the rhombohedral $Sc_{0.1}Ce_{0.01}ZrO_2$ has formed surface termination steps [13]. The formation of the rhombohedral structure has occurred during annealing of the cubic $Sc_{0.1}Ce_{0.01}ZrO_2$ at 375 °C for 12 h which lead to a full transformation from cubic to rhombohedral phase. The confocal optical micrographs of the Vickers impressions obtained by indenting cubic and rhombohedral $Sc_{0.1}Ce_{0.01}ZrO_2$ are shown in Fig. 5(D and C). Total of 20 impressions were made for each sample at a 9.8 N load. The impressions were used for the measurements of hardness and indentation fracture toughness. Thus, $H_v = 14.02 \pm 0.3$ GPa and $K1_C = 2.03 \pm 0.7$ MPa $m^{1/2}$ are reported for cubic $Sc_{0.1}Ce_{0.01}ZrO_2$ and $H_v = 13.78 \pm 0.4$ GPa and $K1_C = 1.68 \pm 0.2$ MPa $m^{1/2}$ are reported for rhombohedral $Sc_{0.1}Ce_{0.01}ZrO_2$.

In order to determine the stability of the cubic and rhombohedral phases in 25–400 °C temperature range the heating/cooling experiments were performed where spectra in the region of 1240–1740 cm^{-1} were collected from three different locations on the sample's surface during heating and cooling. Three different samples of cubic $Sc_{0.1}Ce_{0.01}ZrO_2$ and three different samples of rhombohedral $Sc_{0.1}Ce_{0.01}ZrO_2$ were indented using a Vickers indenter at 9.8 N. For each indented sample, a separate location has been chosen: (a) a non-deformed polished surface far away from the impression; (b) a center of the Vickers impression; (c) a location close to the Vickers impression where a stress should develop due to a deformation introduced by indentation. The last two locations, a center of the Vickers impression and a stress field point, are shown in Fig. 5C.

The spectra collected from three different locations in cubic and rhombohedral phases during heating and cooling up to 400 °C are presented in Fig. 6. It was detected that while cubic phase is retained as cubic on the polished non-deformed surface for the performed heating experiment, it would transform to a rhombohedral structure upon cooling in the center of the Vickers impression, where the mixture of cubic and rhombohedral phases could be detected at room temperature after cooling (Fig. 6A). However, at the stress field (approximate location is shown with a black dot in Fig. 5C) a full transformation from the cubic to rhombohedral phase would occur, thus only the spectrum of rhombohedral phase can be found and no cubic phase can be detected after cooling. At the same time, it was found that the rhombohedral phase is stable in the whole 25–400 °C temperature range at all three locations both upon heating and cooling conditions (Fig. 6B).

The position of the peaks of cubic and rhombohedral phases was analyzed as a function of the locations and temperature (Fig. 7). While the positions of 1329 cm^{-1} peak, of the cubic phase collected from the center of the Vickers impression and the stress field, with the same tendency observed for 1521 cm^{-1}, were shifted to the higher wavenumbers relative to the peak position collected from the polished, non-deformed surface (Fig. 7A), the opposite tendency was detected to occur for some of the peaks of the rhombohedral phase (Fig. 7B). Thus, 1472 cm^{-1} peaks of the rhombohedral phase were shifted to the lower wavenumbers by ~10–15 cm^{-1} relative to their positions at the polished and stress field surfaces, while 1338 cm^{-1} peak of rhombohedral phase hardly showed any shift in position. This difference can be clearly seen when 2D maps of the peak positions were created with Vickers impression made in cubic and rhombohedral phases (Fig. 8). The 2D peak position maps of 1329, 1444, and 1521 cm^{-1} peaks of the cubic $Sc_{0.1}Ce_{0.01}ZrO_2$ along with the representative spectra taken from the location of interest are shown in Fig. 8A. The Raman micrographs of the Vickers impression, created by mapping positions of the 1329 and 1521 cm^{-1} peaks give an indication of where the impression is located and what is the shift of the peaks depending on the location. However, the 1444 cm^{-1} peak shows a homogeneous distribution of the peak position in the region of interest, therefore it is not stress/strain sensitive. The position of the 1329 and 1521 cm^{-1} peaks of the cubic phase shifted to the higher wavenumbers in the center of the Vickers impression, as indicated in Fig. 8A. At the same time the 2D peaks position maps created using 1338, 1472, 1560, and 1642 cm^{-1} peaks of the rhombohedral $Sc_{0.1}Ce_{0.01}ZrO_2$ showed that the shift to the lower wavenumbers occurred in the center of the

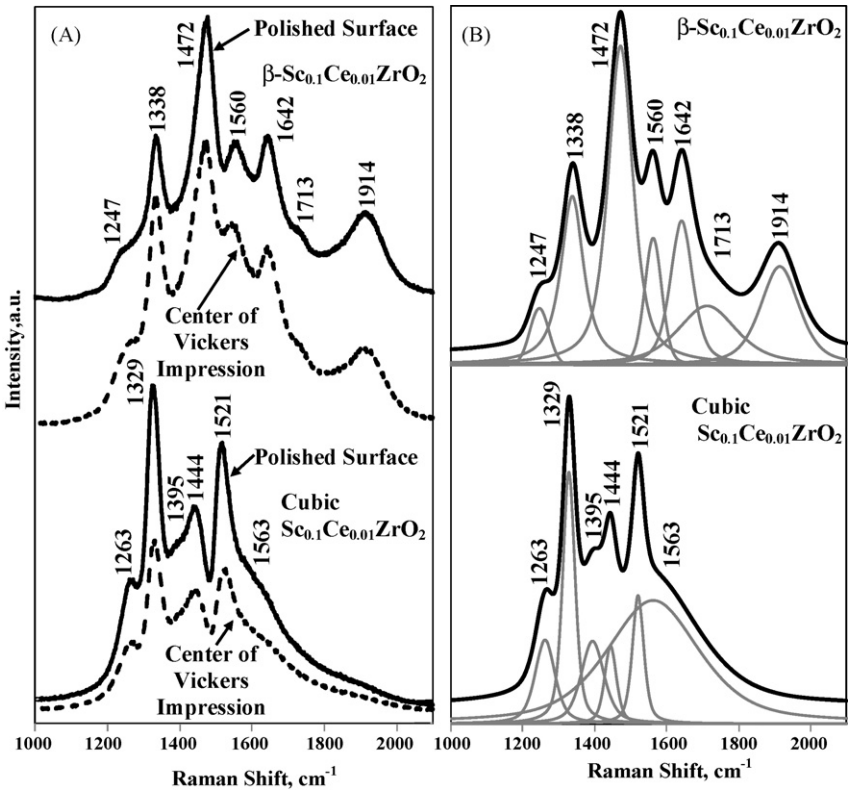

Fig. 4. (A) Typical spectra of cubic and rhombohedral (β) $Sc_{0.1}Ce_{0.01}ZrO_2$ and (B) the deconvoluted peaks of cubic and rhombohedral (β) $Sc_{0.1}Ce_{0.01}ZrO_2$.

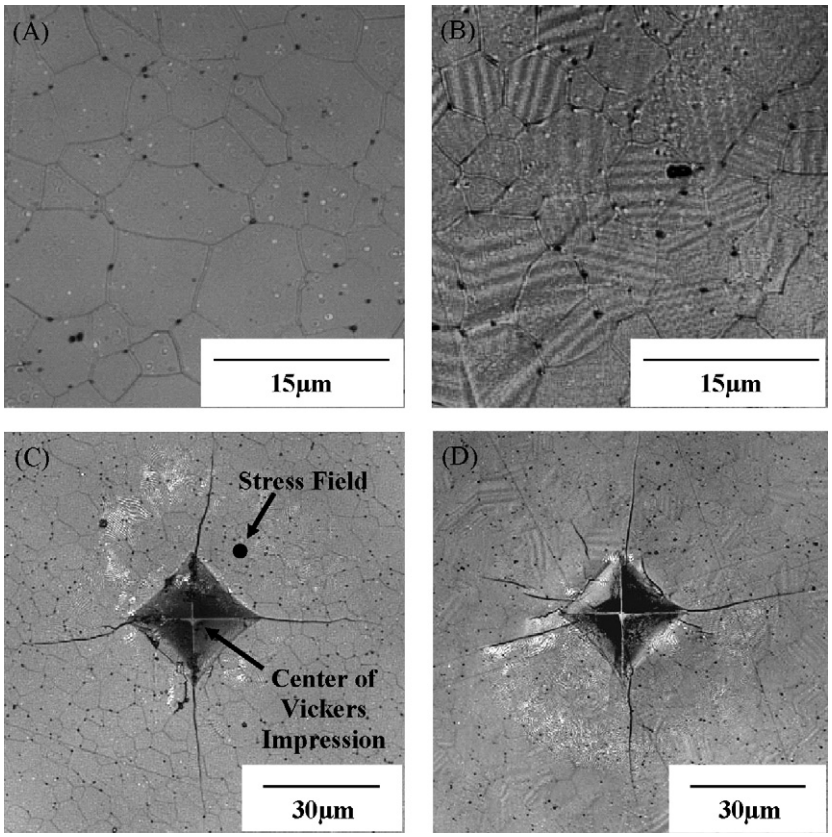

Fig. 5. (A and B) Confocal images of cubic and rhombohedral (β) $Sc_{0.1}Ce_{0.01}ZrO_2$, (C and D) confocal optical micrographs of impressions made by a Vickers indenter in (A) cubic of $Sc_{0.1}Ce_{0.01}ZrO_2$ and (B) rhombohedral (β) $Sc_{0.1}Ce_{0.01}ZrO_2$ ceramics used to determine hardness and indentation fracture toughness, as well as used for mapping experiments.

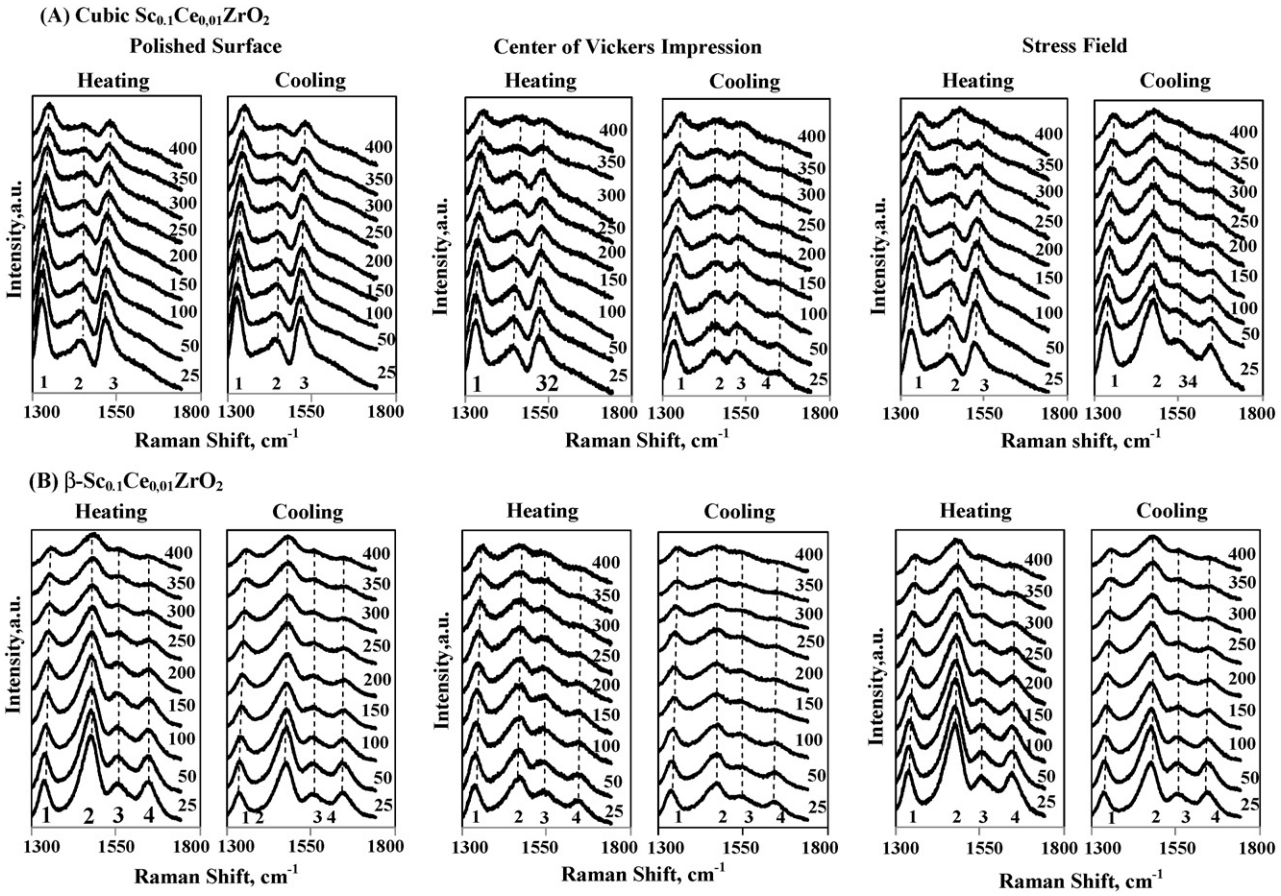

Fig. 6. Spectra of cubic (A) and rhombohedral (B) $Sc_{0.1}Ce_{0.01}ZrO_2$ during heating and cooling up to 400 °C.

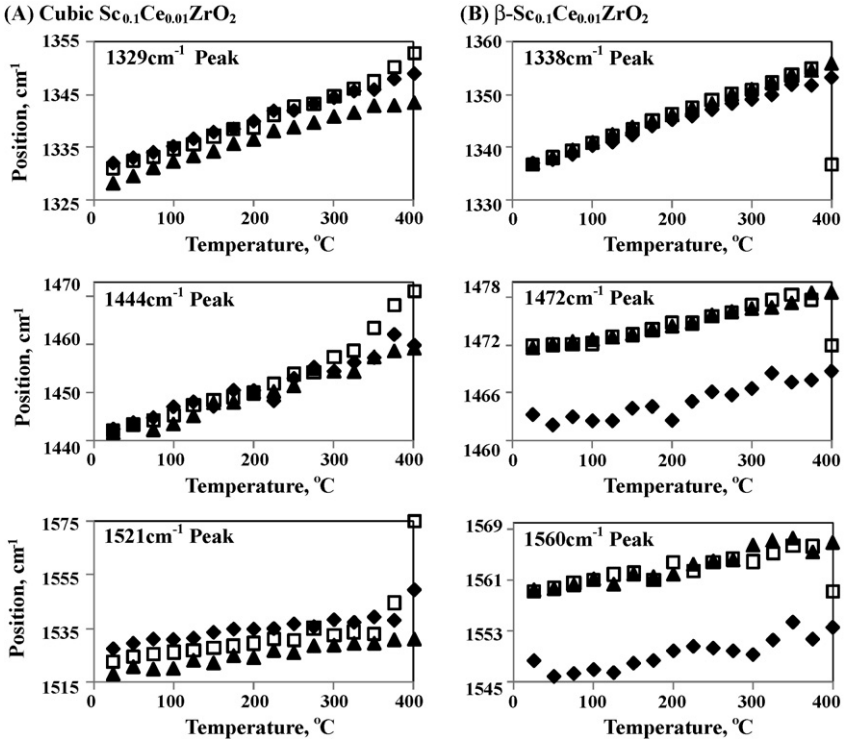

Fig. 7. Position of the peaks of cubic (A) and rhombohedral (β) phases (B) vs. temperature upon heating experiments; (▲) polished surface, (♦) center of Vickers impression, (□) stress field.

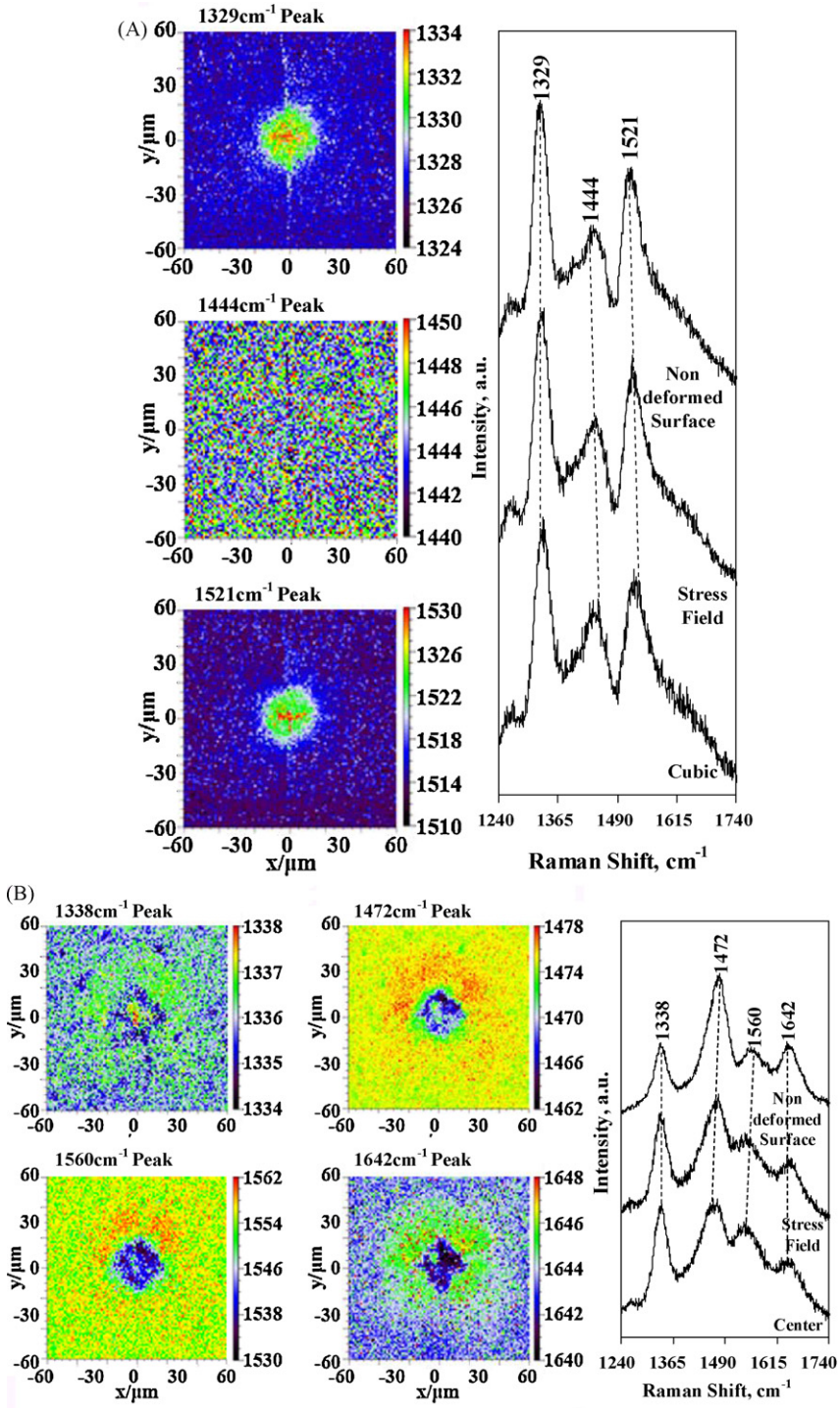

Fig. 8. 2D maps of the positions of peaks for cubic (A) and rhombohedral (B) $Sc_{0.1}Ce_{0.01}ZrO_2$. The typical spectra of the two phases are also presented.

Vickers impression for all four peaks (Fig. 8B). The reason of the shifts to the lower wavenumbers can lie in a different response to the compressive stress of the rhombohedral phase, but it could also be explained by a different response of the particular vibrations under consideration. To explain the differences, the uniaxial stress/strain calibration experiment, for both cubic and rhombohedral phases, are required that will be performed in the future.

After heating/cooling experiments of the cubic phase in 20–400 °C temperature range (Fig. 6) it became clear that not only temperature, but also existing stress affects the phase composition of $Sc_{0.1}Ce_{0.01}ZrO_2$. Fig. 9A shows the confocal optical micrograph of the impression after heating/cooling to 400 °C experiment of the indented cubic $Sc_{0.1}Ce_{0.01}ZrO_2$. The deformation zones formed around impression are clearly visible. This impression was used for mapping (Fig. 9B) which shows formation of the rhombohedral phase in the stressed fields around the impression after heating/cooling. The impression map was created using the area of 180 μm × 180 μm of the impression, presented in Fig. 9A. The typical spectra, corresponding to cubic, rhombohedral and a mixture of two phases, collected from the different locations on the maps are given in Fig. 9B. As one can see from the map (Fig. 9C), the cubic phase was mostly retained both further away outside of the

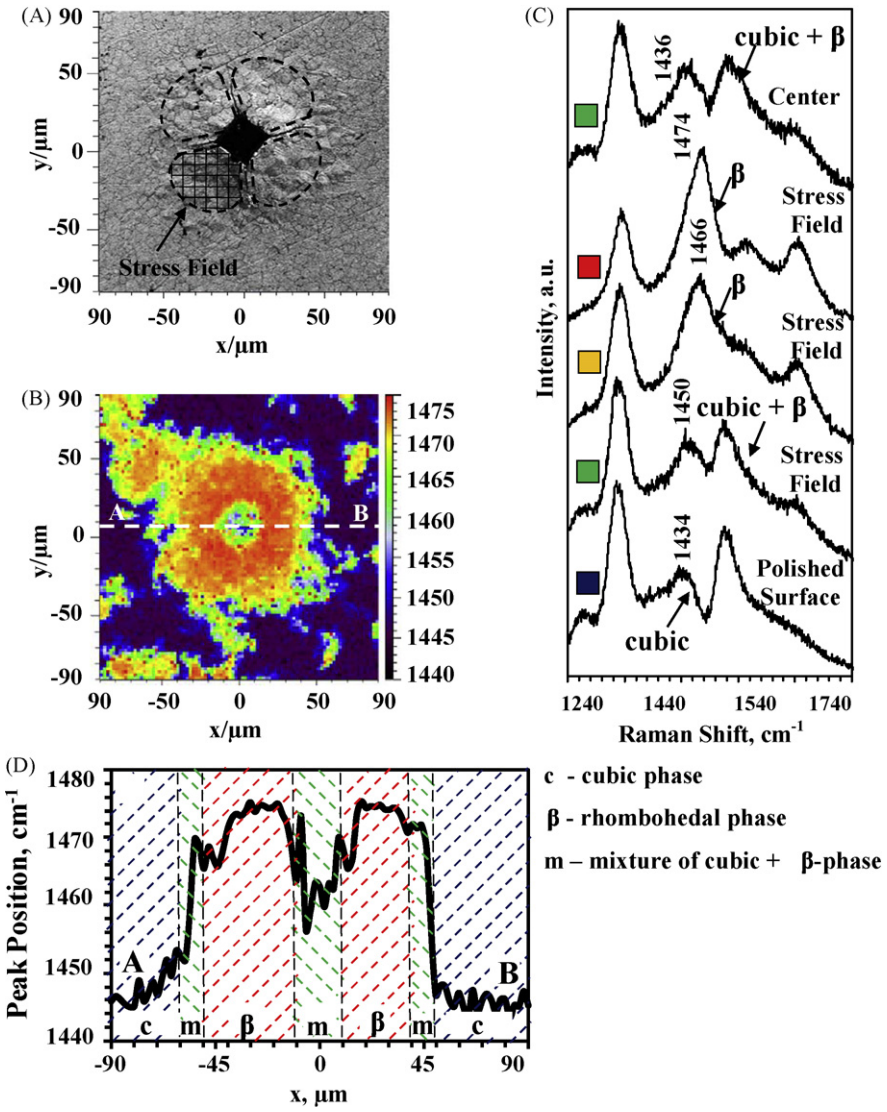

Fig. 9. (A) Confocal micrograph of Vickers impression in cubic $Sc_{0.1}Ce_{0.01}ZrO_2$ phase after 400 °C heating/cooling; The Vickers impression was placed before heating/cooling. (B) 2D maps of 1434–1474 cm^{-1} peak position of the selected area with the Vickers impression and deformation zones corresponding to the micrograph from (A); (C) typical spectra corresponding to cubic, cubic + rhombohedral (β), and pure rhombohedral (β) phases from three different locations of the map presented in 9B; (D) 1D map of the 1430–1480 cm^{-1} peak position collected along *x*-axis at the intersection with 0 of *y*-axis along AB line.

deformation zone at the polished surface and inside of the Vickers impression after heating/cooling, however the cubic to rhombohedral phase transformation has occurred inside of the stress field. The 1D line map of the ~1460 cm^{-1} peak position along the *x*-axis from A to B shown in Fig. 9D. It shows that the peak position of the cubic phase inside the Vickers impression has shifted to the higher wave numbers relative to the non-deformed cubic phase which is located outside of the impression. The separate zones, containing either almost pure cubic or rhombohedral phase or a mixture of cubic and rhombohedral phases, are highlighted with relevant dashed lines. A cubic phase was found outside the Vickers impression and deformation zone surrounding impression, a rhombohedral phase was mostly found within a deformation zone, and a mixture of cubic and rhombohedral phases was found within the impression, but also in the narrow interval at the outside area of the deformation zone (Fig. 9D).

4. Conclusions

The effect of the temperature and stress on the stability of the cubic and rhombohedral $Sc_{0.1}Ce_{0.01}ZrO_2$ ceramics has been studied by micro-Raman spectroscopy. The whole spectral range of the cubic and rhombohedral $Sc_{0.1}Ce_{0.01}ZrO_2$ collected using 532 and 785 nm lasers has been reviewed. The bands located at 239, 480, and 623 cm^{-1} are detected by using two available lasers. However, most of the bands can only be seen by using either 532 or 785 nm lasers. Such bands can be tentatively assigned to the appearance of the luminescence peaks related to $Ln3^+$ impurity ions and further photoluminescence study is required to determine the nature of the impurities responsible for the appearance of the bands.

The phase stability of the cubic and rhombohedral phases has been studied by in situ heating experiment. It was found that the cubic phase is stable upon heating up to 1000 °C using fast heating/cooling rates (10 °C min^{-1}) in the experiment. The rhombohedral $Sc_{0.1}Ce_{0.01}ZrO_2$ is stable upon heating in 25–400 °C temperature range. The cubic to rhombohedral phase transformation can be detected when cubic $Sc_{0.1}Ce_{0.01}ZrO_2$ was deformed by an indentation and then heated up to 400 °C. Upon cooling from 400 °C to room temperature, the cubic phase transformed to the rhombohedral phase if located near to the Vickers impression. Thus, it is not only the temperature but also the introduced stress which are responsible for facilitating of the cubic to rhombohe-

dral phase transition upon cooling. While it might be difficult to determine the stress distribution around the Vickers impressions in $Sc_{0.1}Ce_{0.01}ZrO_2$, due to complexity of the stress state, an uniaxial compression experiments are required to determine the stress sensitivity and piezospectroscopic coefficients of the bands in cubic and rhombohedral phases. However, based on the present finding it is clear that both applied stress and heating of the material within a certain temperature range will promote a cubic to rhombohedral phase transition in $Sc_{0.1}Ce_{0.01}ZrO_2$.

The mapping experiments were performed to collect the preliminary data, such as a shift of the selected peaks, which can be further used to characterize stress states or detect any possible phase transition in the materials indented by Vickers. The stress related shift of peak positions has been detected both in cubic and rhombohedral $Sc_{0.1}Ce_{0.01}ZrO_2$ upon indentation. The peaks under investigation were shifted to the higher wavenumbers in the center of the Vickers impression in the cubic phase; however most of the investigated peaks of the rhombohedral $Sc_{0.1}Ce_{0.01}ZrO_2$ were shifted to the lower wavenumbers in the center of the impression. Further studies are required to determine the origin of the bands and establish a dependence of their positions on the applied stress. However, even without quantification of the complex stress state around the impression one can say that in order to promote cubic to rhombohedral phase transition in $Sc_{0.1}Ce_{0.01}ZrO_2$ both temperature and applied stress are required.

Acknowledgement

This work was supported by the NSF DMR project number 0502765.

References

[1] Z. Ze, Q. Zhu, Solid State Ionics 176 (2005) 2791–2797.
[2] I. Kosacki, H.U. Anderson, Y. Mizutani, K. Ukai, Solid State Ionics 152/153 (2002) 431–438.
[3] V. Kharton, F.M.B. Marques, A. Atkinson, Solid State Ionics 174 (2003) 135–149.
[4] S.P.S. Badwal, S.F. Ciacehi, S. Rajendran, J. Drennan, Solid State Ionics 109 (1998) 167–186.
[5] O. Yamamoto, Y. Arachi, Y. Takeda, N. Jmaniski, Y. Mizutani, M. Kawai, Y. Nakanmra, Solid State Ionics 79 (1995) 127–142.
[6] Y. Arachi, Y.M. Sakai, Y. Yamamoto, Y. Takeda, N. Imaniski, Solid State Ionics 121 (1999) 133–139.
[7] H. Yananura, N. Utsunomiya, T. Mari, T. Ateka, Solid State Ionics 107 (1998) 185–189.
[8] V. Arachi, T. Asai, O. Yamamoto, V. Takeda, N. Imaniski, K. Kawate, C. Tamakoshi, J. Electrochem. Soc. 148 (2001) A520–A523.
[9] M. Yashima, T. Kakihana, M. Yoshimura, Solid State Ionics 86–88 (1996) 1131–1149.
[10] H. Fuijimori, M. Yashima, M. Kakihana, M. Yoshimura, J. Appl. Phys. 91 (2002) 6493–6498.
[11] D.S. Lee, W.S. Kim, S.H. Choi, J. Kim, H.W. Lee, J.H. Le, Solid State Ionics 176 (2005) 33–39.
[12] Z. Wang, N. Chang, Z. Bi, Y. Dong, H. Zhang, J. Zhang, Z. Feng, C. Li, Mater. Lett. 59 (2005) 2579–2582.
[13] S. Yarmolenko, J. Sanker, J. Bernier, N. Klimov, N. Kapat, J. Orlovskaya, J. Fuel Cell Sci. Technol. 6 (2009) 1–8, 021007.
[14] A. Zevalkink, A. Hunter, M. Swanson, C. Johnson, J. Kapat, N. Orlovskaya, Mater. Res. Soc. Symp. Proc. 972 (2007).
[15] N. Orlovskaya, S. Lukich, G. Subhash, T. Graule, J. Kuebler, J. Pow. Sourc. (2009) in press, doi:10.1016/j.jpowsour.2009.11.016.
[16] S. Lukich, C. Carpenter, N. Orlovskaya, in: D. Singh, J. Salem (Eds.), Proceedings of the 33th International Conference on Advanced Ceramic and Composites, WILEY, 2009, pp. 4–14.
[17] T. Otake, H. Yugami, H. Naito, K. Kawanmra, T. Kawada, J. Mizusaki, Solid State Ionics 135 (2000) 663–667.
[18] V.M. Orera, R.I. Merino, F. Pena, Solid State Ionics 72 (1994) 224–231.
[19] J. Kaspar, P. Fornasiero, G. Baldueci, R. Di Monte, N. Hickey, V. Sergo, Inorg. Chim. Acta 349 (2003) 217–226.
[20] N. Maczka, E.T.G. Lutz, H.J. Verbuk, K. Oskam, A. Meijerink, J. Hanuza, N. Stuivinga, J. Phys. Chem. Solids 60 (1999) 1909–1914.
[21] I.N. Asher, B. Papanicolaou, E. Anastassakis, J. Phys. Chem. Solids 37 (1976) 221–225.
[22] P. Fornasicro, A. Spghini, R. Di Monte, M. Bettinelli, J. Kaspar, A. Bigotto, V. Sergo, M. Graziani, Chem. Mater. 16 (2004) 1938–1944.
[23] H. Kishimoto, N. Sakai, T. Horita, K. Yamaji, Y.P. Xiong, M.E. Brito, H. Yokokawa, Solid State Ionics 179 (2008) 2037–2041.
[24] G. Vlaic, R. Di Monte, P. Fornasiero, E. Fonda, J. Kaspar, M. Graziani, J. Catal. 182 (1999) 378–389.
[25] M. Yashima, H. Arashi, N. Kakihana, M. Yoshimura, J. Am. Ceram. Soc. 77 (1994) 1067–1071.
[26] C.M. Philippi, K.S. Mazgiyasni, J. Am. Ceram. Soc. 54 (1971) 254–258.
[27] A. Feinberg, C.H. Perry, J. Phys. Chem. Solids 42 (1981) 513–518.
[28] I. Kosacki, V. Petrovsky, H. Anderson, P. Colomban, J. Am. Ceram. Soc. 85 (2002) 2646–2650.
[29] A. Limarga, D. Clarke, J. Am. Ceram. Soc. 90 (2007) 1272–1275.
[30] R.F. Wallis, A.A. Maradudin, Phys. Rev. 125 (1962) 1277–1282.
[31] S. Raghavan, P.K. Imbrie, W. Crossley, Appl. Spectrosc. 62 (2008) 765–1765.
[32] S. Raghavan, P.K. Imbrie, J. Am. Ceram. Soc. 92 (2009) 1567–1573.